Journal of Solid State Chemistry **156,** 428–436 (2001)
doi:10.1006/jssc.2000.9018, available online at http://www.idealibrary.com on IDEAL®

The Fine Structure of $YCuO_{2+x}$ Delafossite Determined by Synchrotron Powder Diffraction and Electron Microscopy

G. Van Tendeloo,*,[1] O. Garlea,† C. Darie,† C. Bougerol-Chaillout,† and P. Bordet†

*EMAT, University of Antwerp, Groenenborgerlaan 171, B-2020 Antwerp, Belgium; and †CNRS, Laboratoire de Cristallographie, BP 166X, 38042 Grenoble Cedex 9, France

Received July 12, 2000; in revised form October 16, 2000; accepted October 27, 2000

$YCuO_2$ delafossite crystallizes into two stacking variants; hexagonal 2H or rhombohedral 3R, depending on the preparation conditions. The structure of the fully oxygenated material $YCuO_{2.50}$ has been determined as orthorhombic ($a_o = 6.1961$ Å; $b_o = 11.2158$ Å; $c_o = 7.1505$ Å; space group *Pnma*). The structure is based on the hexagonal 2H structure ($a_o = a_H\sqrt{3}$; $b_o = c_H$; $c_o = 2a_H$). Upon incomplete oxidation, a different $YCuO_Z$ phase with ideal composition $YCuO_{2.33}$ and lattice parameters $a_H\sqrt{3}$, $a_H\sqrt{3}$, c_H is also formed. Diffraction patterns are often very complex because of the presence of planar defects and intergrowth of both phases. Under electron beam irradiation, oxygen is released from the structure and one phase gradually transforms into the other. © 2001 Academic Press

Key Words: **delafossite; X-ray diffraction; electron microscopy; oxygen ordering.**

1. INTRODUCTION

Delafossites of the type $LnCuO_{2+x}$ (Ln = Y or La) have been studied in fair detail by Cava *et al.* (1). The basic structural formula is $A^{1+}B^{3+}O_2$, where the A^{1+} is always Cu^{1+} in the present case. The structure can be described as a succession of LnO_2 layers, with the Ln in octahedral coordination and where neighboring octahedra share edges, so as to form a hexagonal arrangement of Ln. Successive LnO_2 layers are connected by a Cu plane, where the Cu is in a linear stick coordination with the oxygens above and below (see Figs. 1 and 2 in (1)). These double-layer (LnO_2–Cu) sandwiches with a thickness of 5.6 Å can be stacked in different ways, creating a number of polytypes (2, 3). $LaCuO_2$ for example shows a 3R stacking (2) while $YCuO_2$ has a 2H stacking (3). High-resolution electron microscopy (HREM) observations of Cava *et al.* (1) show a large variety of stacking variants for $YCuO_2$, which apparently points toward a low stacking fault energy and a small stacking energy difference between the different phases.

Delafossites of the type $LaCuO_2$ and $YCuO_2$ are also known to easily intercalate extra oxygen in the Cu planes, leading to a structural formula of the type $LnCuO_{2+x}$ (x being of the order of 0.5). These oxygens tend to adopt an ordered arrangement within the CuO_x plane and give rise to different superstructures (see (1)). This oxygen ordering affects the symmetry within the plane and lowers the space-group symmetry; two of these superstructures have been identified by Cava *et al.* (1), one being orthorhombic with lattice parameters $2a$, $a\sqrt{3}$, c, and the other being hexagonal but with lattice parameters $a\sqrt{3}$, $a\sqrt{3}$, c. TEM revealed the presence of several planar defects and phases with a different superstructure. These effects hampered a direct interpretation of the diffraction patterns and no detailed structure could be proposed.

The idea of this contribution is to study the different $YCuO_{2+x}$ structure(s) in more detail by X-ray diffraction, electron diffraction, and HREM and to relate the different oxygenated materials. A basic requirement, however, is to be able to prepare homogeneous, single-phase samples.

2. EXPERIMENTAL

A polycrystalline sample of $YCuO_2$ delafossite was prepared by solid-state reaction technique. The difficulty of this synthesis consists in isolating the 3R and 2H polytypes of $YCuO_2$. These polytypes are very often intergrown probably due to a very small difference in the thermodynamical stability region of these two phases.

As a common first step, the $Y_2Cu_2O_5$ precursor was synthesized from reagent grade Y_2O_3 and CuO. The starting materials were mixed by grinding in a mechanical mortar for 1 h and the powder mixture was fired in air at 1050°C for 1 day.

To obtain high-purity powder of the 2H phase, the calcinated $Y_2Cu_2O_5$ powder was pressed into pellets and buried in powder of the same composition. This product put in

[1]To whom correspondence should be addressed.

0022-4596/01 $35.00

Al_2O_3 crucibles was heated at 400°/h to 1134°C in air, annealed in flowing Ar for 1 h, and cooled to room temperature in the gas stream. The resulting pellets were then powderized and the excess copper oxide was removed by leaching in aqueous ammonia for 2 days. This method reproducibly yielded single phase $YCuO_2$ (2H).

To determine the temperature range in which $YCuO_2$ (3R) can be synthesized, samples of $Y_2Cu_2O_5$ (pellets buried in powder in Al_2O_3 crucibles) were inserted into a gradient furnace spanning the temperature range 1170–1210°C in flowing Ar for 2 h. The samples were analyzed by X-ray powder diffraction. The results show that single-phase 3R can be synthesized only in a very narrow temperature range, between 1190 and 1200°C. Above 1200°C, 3R-$YCuO_2$ is never found as a single phase but as part of a multiphase mixture which consists of 3R-$YCuO_2$, Cu_2O, and Y_2O_3. Below 1190°C a two-phase mixture (2H-$YCuO_2$ and 3R-$YCuO_2$) is obtained. Therefore, successful synthesis of the 3R-$YCuO_2$ phase requires fast heating into the temperature stability region to prevent the formation of 2H-$YCuO_2$.

In order to produce the bulk delafossite-derived oxides, $YCuO_{2+\delta}$, pieces of a polycrystalline pellet, 2H-$YCuO_2$, were heated at 460°C for 15 h in flowing oxygen. The oxygen content was determined by a thermogravimetric hydrogen reduction method, heating to 1000°C and measuring the weight loss according to the reaction: $YCuO_{2+\delta} \rightarrow 0.5\ Y_2O_3 + Cu + 0.5\ (\delta + 0.5)O_2$. The oxygen content in this case reached 2.52(3)/F.U.

The samples were characterized by X-ray powder diffraction using a Siemens D5000 diffractometer in transmission geometry, with Cu$K\alpha$1 radiation selected by a focusing Ge(111) monochromator. The synchrotron powder diffraction experiment was carried out at room temperature at the BM16 beam line of the ESRF, Grenoble, using a glass capillary of 0.7 mm in diameter. The monochromatic X-rays (wavelength 0.4454 Å) were selected with a double-crystal Si(111) monochromator, and detection was performed with the nine-crystal multianalyzer stage installed on the BM16 diffractometer. The data collected with the nine detectors were corrected for beam monitor variations and $\approx 2°$ angular shift between the analyzer crystals, summed, and rebinned to a 0.0025 2θ step size.

For electron microscopy, samples were crushed and deposited onto a carbon-coated copper grid. TEM observations were made in a Philips CM300 and a Jeol 4000EX. Oxygen ordered superstructures of $YCuO_{2+\delta}$ turned out to be radiation sensitive and minimum exposure techniques had to be used to obtain HREM images of the fully oxygenated phase.

3. RESULTS

3.1. $YCuO_2$

As discussed in the previous section, depending on the preparation conditions, stoichiometric $YCuO_2$ samples can crystallize into two different stacking modes: the rhombohedral 3R structure or the hexagonal 2H structure. Evidence for the occurrence of both structures in pure form can be found in the electron diffraction patterns of Figs. 1 and 2, respectively. Most diffraction patterns do not show any streaking along the c^*-direction, pointing toward perfect stacking sequences with no, or a limited number of, stacking errors. This is different from the results presented in (1), where invariably a large number of stacking faults and twin boundaries were observed. If the preparation temperature is not perfectly controlled, a mixture of 2H, 3R and a number of intermediate stacking sequences results. The stacking sequence can be directly visualized from the HREM image along the [11.0] zone of the 2H polytype (Fig. 3). Under the defocus conditions used, Cu atoms are imaged as bright dots, situated in the (00.1) mirror planes; the in-between bright dots correspond to the Y-positions. Note that in this section, no effect of any eventual ordering of oxygens in the Cu–O plane is to be expected; this will be discussed in the next section.

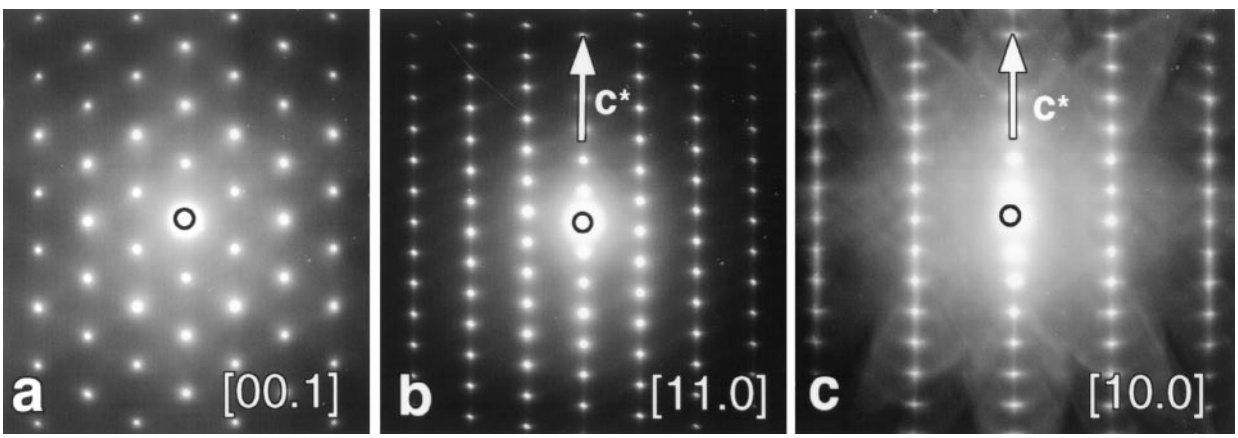

FIG. 1. Electron diffraction patterns of $YCuO_2$ (3R variant) along the three main sections [00.1], [11.0], and [100].

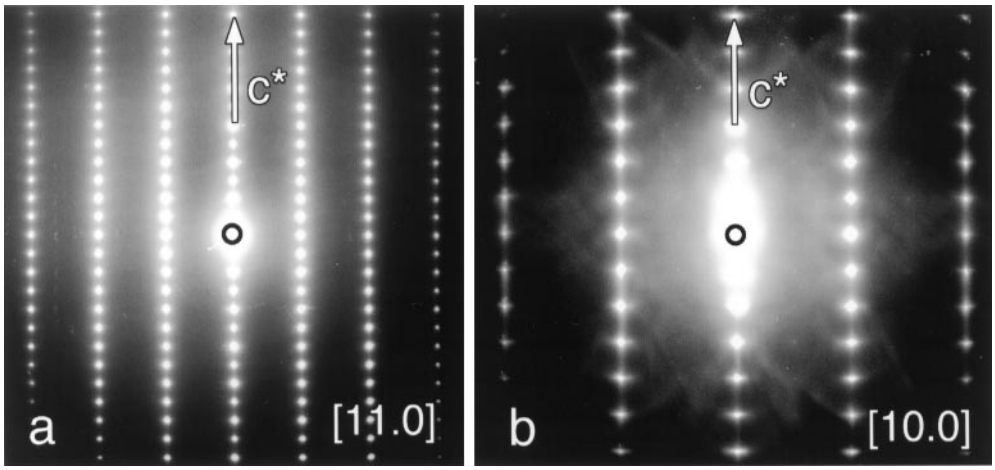

FIG. 2. Electron diffraction patterns of $YCuO_2$ (2H variant) along [11.0] and [100].

3.2. $YCuO_{2.50}$

All oxygenated $YCuO_{2.50}$ samples considered here (prepared under the conditions described in section 2) show the basic 2H structure with $a \approx 3.5$ Å and $c \approx 11.2$ Å; only occasionally a stacking fault, locally creating the 3R structure, is present. The most striking, however, is the presence of different superstructure reflections. This is particularly striking in the $[10.0]_H$ section. In Fig. 4 we have gathered a collection of different patterns; all corresponding to the basic $[10.0]_H$ section. In (1) a number of these patterns have also been observed, but no structure description has been given. We have found that these superstructures (and even others) occur in different parts of the sample and moreover that electron beam irradiation can alter the positions of the superstructure reflections. Below we will try to identify the different phenomena.

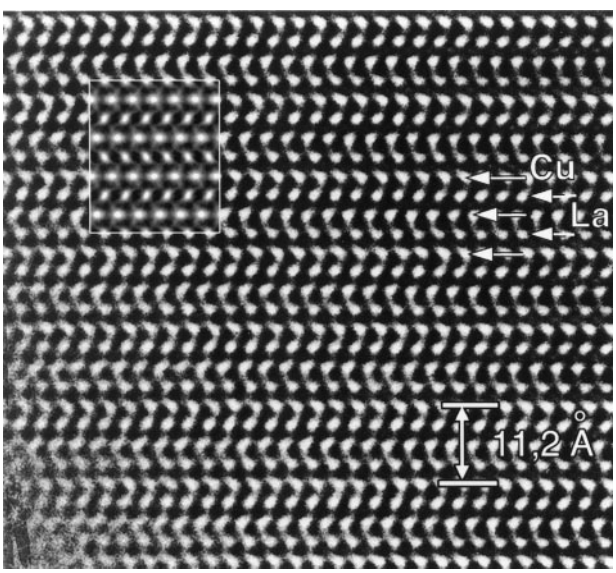

FIG. 3. HREM image of the perfect stacking of $YCuO_2$ along the [11.0] zone. A calculated image for a defocus of 700 Å and a thickness of 84 Å is shown as an inset.

Careful preparations, however (see section 2), make it possible to obtain single-phase, fully oxygenated, $YCuO_{2.50}$ material. Three representative electron diffraction patterns of this phase, taken without intense electron beam irradiation, are shown in Fig. 5. The structure can be perfectly described in an orthorhombic unit cell with approximate lattice parameters $a_o = 6.2$ Å; $b_o = 11.2$ Å; $c_o = 7.2$ Å. This unit cell is closely related to the hexagonal 2H lattice parameters of the nonoxygenated compound ($a_o = a_H\sqrt{3}$; $b_o = c_H$; $c_o = 2a_H$). Extinctions are observed for $00l$ ($l = 2n + 1$), $h00$ ($h = 2n + 1$), $0k0$ ($k = 2n + 1$), $0kl$ ($k + l = 2n + 1$) and $hk0$ ($h = 2n$); in agreement with a *Pnma* spacegroup. The diffraction patterns in Fig. 5 can therefore be identified as $[010]_o = [00.1]_H$, $[001]_o = [11.0]_H$, and $[100]_o = [10.0]_H$. It should be noted that no oxygen ordering is observed along the $[001]_o$ pattern (Fig. 5b) and that the $[010]_o$ section in Fig. 5a contains two orientation variants. The $0k0$ reflections with k odd are present due to double diffraction. This is clear from tilting experiments along the b_o* axis ; $0k0$ reflections with k odd then disappear.

Based on the *Pnma* space group determined from electron diffraction data, the structure was solved by direct methods, using the program EXPO (4), and then further refined by the Rietveld technique with the WinPLOTR software (FullProf 99) (5). EXPO used in default mode readily led to a complete structure solution (cfom = 0.999, $R = 7.45\%$), with yttrium and two oxygen atoms in general $8d$ positions, and two copper and one oxygen atoms in the $y = \frac{1}{4}$ $4c$ special positions. These positions were introduced as a starting model

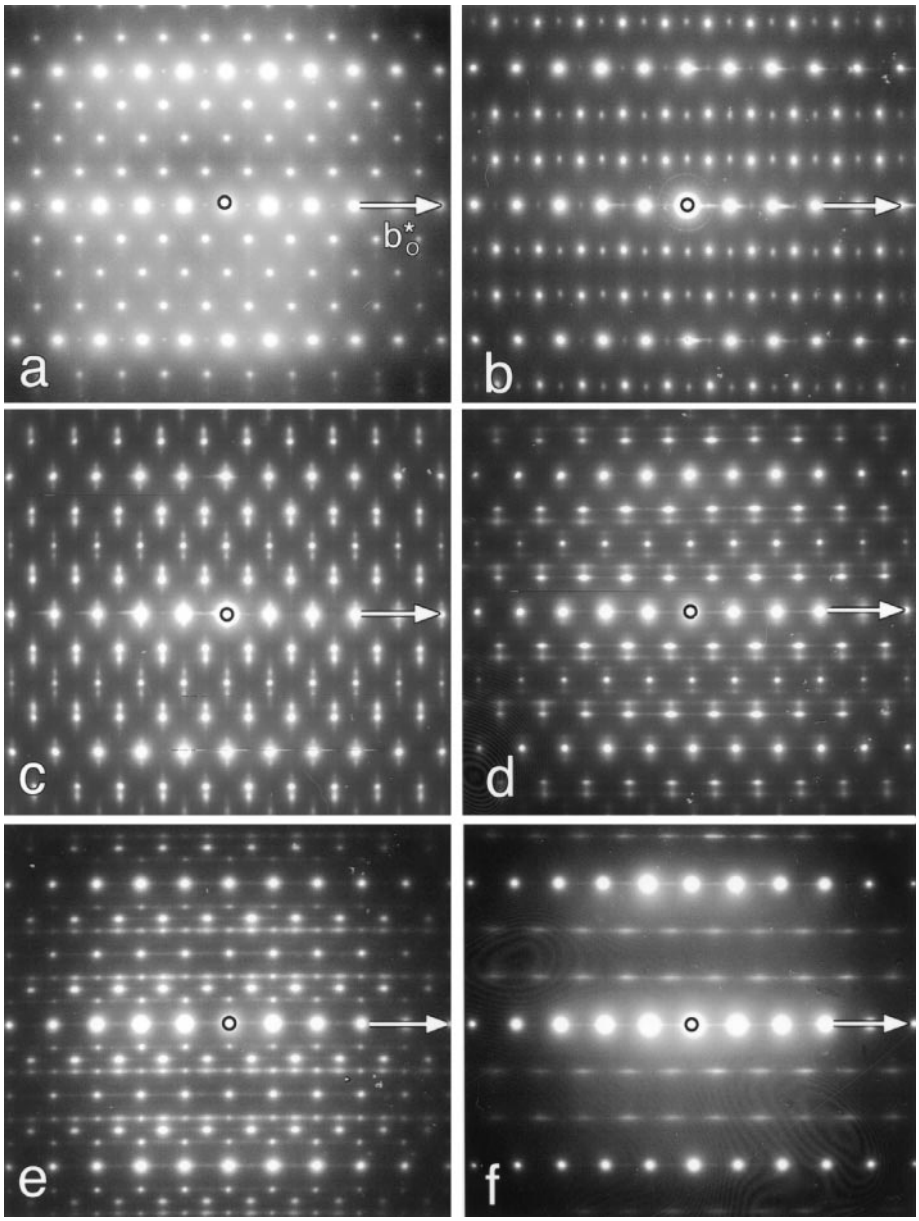

FIG. 4. Different diffraction patterns of oxidized material, corresponding to the basic $[10.0]_H$ pattern (Fig. 1c). Note the different arrangements of the superstructure reflections.

in the Rietveld refinement. The data were corrected for absorption. The background was described by a fifth-order polynomial. A pseudo-Voigt peak shape was used, and the widths of the Bragg peaks were described with the Thomson–Cox–Hastings function. The minimum full width at half maximum of the peaks was $\approx 0.03^\circ$, but some anisotropic dependence of the peak width was clearly observed. It was taken into account by using an anisotropic uniaxial peak shape dependence, with principal direction along [010] for which the reflection were systematically narrower. This anomalous behavior of the peak shapes is very probably related to the presence of stacking faults and other types of defects present in the sample, as observed by HREM (see below). Refinement of the profile, positional and isotropic thermal parameters lead to a satisfactory convergence with $X^2 = 2.79$ and $R_{\text{Bragg}} = 3.88\%$. Attempts to refine the occupancies of the cations as well as of the anions did not lead to an improvement of the fit, nor to a significant deviation from full occupancy. Difference Fourier syntheses also did not reveal the presence of other oxygen positions in the copper planes, confirming the $YCuO_{2.5}$ stoichiometry for this compound. The structural parameters and principal

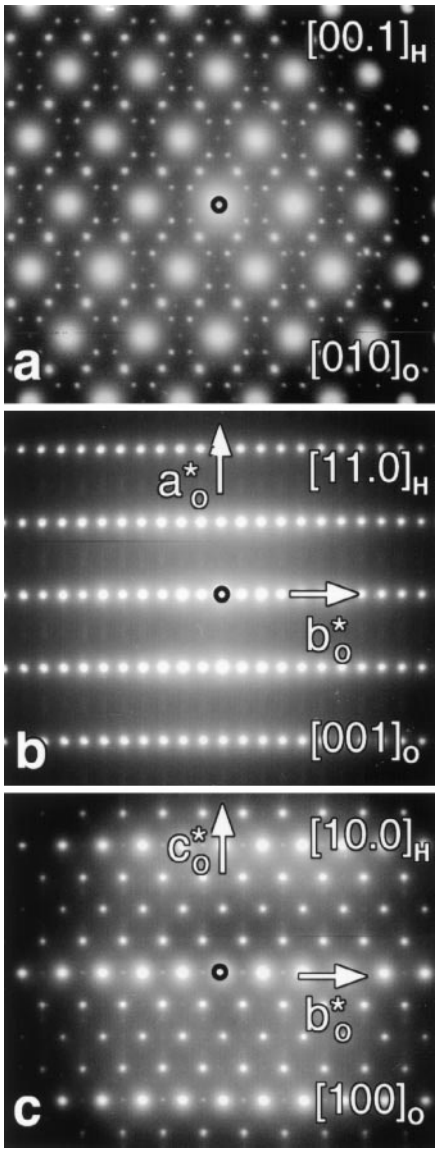

FIG. 5. $[010]_o$, $[001]_o$, and $[100]_o$ electron diffraction patterns of the orthorhombic $YCuO_{2.5}$ superstructure.

interatomic distances are reported in Tables 1 and 2. The quality of the fit is shown in Fig. 6. The values of the isotropic temperature factors for the anions is systematically lower than expected. This is probably a consequence of the defaults present in the sample and of the subsequent imperfection in modelizing the anisotropic reflexion peak shapes.

The structure can be described as a small distortion of the 2H arrangement, brought about by the introduction of the O1 oxygen anions in the copper layers. As shown in Fig. 7, these anions are located at the center of the copper triangles, which share corners to form undulating chains running along the *a*-axis direction. With this arrangement, only one half of the available oxygen sites in the copper layers are occupied, leading to a $CuO_{0.5}$ stoichiometry. The layer is flat by symmetry, but nevertheless slightly distorted, since the copper triangles which accommodate a O1 anion are smaller than those which do not (average Cu–Cu distances: 3.44 and 3.71 Å, respectively).

TABLE 1
Structural Parameters for $YCuO_{2.5}$ Obtained by Rietveld Refinement for Space Group *Pnma* (Cell parameters: $a = 6.1958(2)$, $b = 11.2160(1)$, $c = 7.1508(3)$)

Atom	Position	x	y	z	B_{iso}
Y1	8*d*	0.7535(4)	0.02168(6)	0.1212(2)	0.74(2)
Cu1	4*c*	0.0697(9)	$\frac{1}{4}$	0.1472(4)	0.95(5)
Cu2	4*c*	0.5920(9)	$\frac{1}{4}$	0.8796(4)	0.88(4)
O1	4*c*	0.743(4)	$\frac{1}{4}$	0.108(1)	0.1(2)
O2	8*d*	0.107(2)	0.0864(4)	0.111(1)	0.1(2)
O3	8*d*	0.578(2)	0.0904(4)	0.847(1)	0.0(2)

Note. Agreement factors: R_p, 11.7; R_{wp}, 14.0; R_{exp}, 8.36; χ^2, 2.79. Bragg R factor, 3.88. R_f factor = 2.45.

The coordination of Cu1 is a distorted tetrahedron, with two O1 anions in the copper layer and two O2 anions. These tetrahedra share O1 to form undulating chains along the *a* axis directions. More surprisingly, the Cu2 cation adopts a triangular coordination with one O1 and two O3. The existence of this quite unusual coordination for Cu^{2+} cations is nevertheless clearly demonstrated here.

Figure 8 represents the projection of the structure along the *a*-axis direction. The presence of O1 in the copper layers also induces a distortion of the yttrium environment, which from octahedral in $YCuO_2$ becomes seven-coordinated in $YCuO_{2.5}$, one face of the octahedron being capped by O1 at a distance of 2.56 Å. As a consequence, the yttrium cations move along the *b*-axis toward O1, producing an undulation of the yttrium layers visible in Fig. 8.

The formal cation valences were calculated by using the bond valence sum technique, with the constants reported in (6). The results are given in Table 2. The calculated valences

TABLE 2
Principal Interatomic Distances and Angles and Calculated Cation Valences for $YCuO_{2.5}$

Y1–O1	2.563(1)	Cu1–O1	2.04(2)	Cu2–O1	1.88(1)
–O2	2.31(1)	–O1	2.05(1)	–O3	1.808(4) (2×)
–O2	2.24(1)	–O2	1.867(5) (2×)	Cu2 valence:	1.99
–O2	2.231(9)	Cu1 valence:	1.94		
–O3	2.37(1)	O1–O1	3.70(3)	O1–O3	2.78(1)
–O3	2.296(9)	–O2	2.91(2)	O3–O3	3.582(6)
–O3	2.42(1)	–O2	2.85(1)	O1–Cu2–O3	98°(1)
Y1 valence:	2.96	O2–O2	3.669(6)	O3–Cu2–O3	164°(1)
		O1–Cu1–O1	129°(1)		
		O2–Cu1–O2	159°(1)		

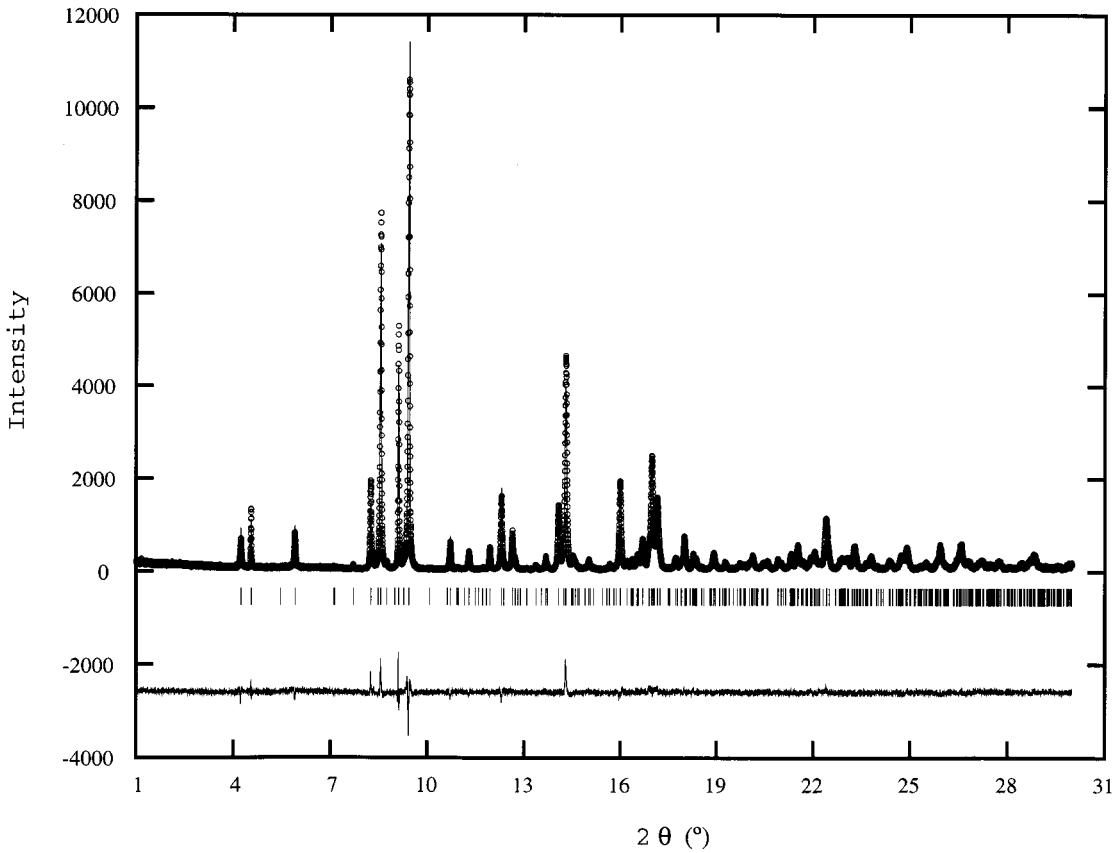

FIG. 6. Rietveld refinement plot of $YCuO_{2.5}$.

of the Y, Cu1, and Cu2 cations are very close to the expected values of $3+$ and $2+$, respectively. Despite the different coordinations of the two copper cations, there is no apparent charge ordering between the two sites. Therefore, this compound realizes an almost regular triangular lattice of spin 1/2 Cu^{2+} cations, which could display quite interesting magnetic properties.

Direct space high-resolution observations were made along all three $\langle 100 \rangle$ orthorhombic sections. As discussed before, the $[001]_o$ section does not reveal the ordering and the HREM image is very similar to the one shown in Fig. 3 for the 2H-$YCuO_2$ sample. The $[100]_o$ zone (Fig. 9) is the most instructive one, particularly when discussing defect structures (see below). The effect of the oxygen insertion is clearly visible, particularly in the "thicker" crystal parts (right side of Fig. 9). Intense dots clearly define a superstructure unit cell of 11.2×7.2 Å (outlined) and according to the calculated images these intense dots correspond to the oxygen configuration in the Cu–O plane. In the thinner parts of the crystal the oxygen ordering is less visible; this is partially because of the reduced thickness but certainly also because of the oxygen disordering due to the electron beam irradiation. In the CuO plane indicated by a single arrow, the ordering is visible all along the line, down to the thin areas, whereas in the neighboring CuO plane, indicated by a double arrow the ordering is visible only in the thicker parts. Because of the oxygen loss and/or disordering, images such as Fig. 9 are hard to obtain and low exposure techniques should be used. Along the $[010]_o$ section the effect of the oxygen ordering is also visible, though much weaker because the heavy cations overlap with the oxygen positions.

3.3. $YCuO_{2+x}$

In Fig. 4 we gathered $[100]_o^*$ sections with a different arrangement of the superstructure reflections. In the pattern of the fully oxidized $YCuO_{2.50}$ (Fig. 4a) the distance between the origin and the 004_o (i.e., the 11.0_H reflection) is subdivided into four spaces by three rows of superlattice reflections. In Fig. 4b this distance between the origin and the basic 11.0_H reflection is separated only by two superlattice rows. This points toward the $a_H\sqrt{3}$, $a_H\sqrt{3}$, c_H superstructure, already mentioned in (1). From the knowledge of the $YCuO_{2.50}$ structure and from symmetry considerations the atom arrangement in this new hexagonal structure with ideal composition $YCuO_{2.33}$ can be easily derived; it is represented schematically in Fig. 10, using space group

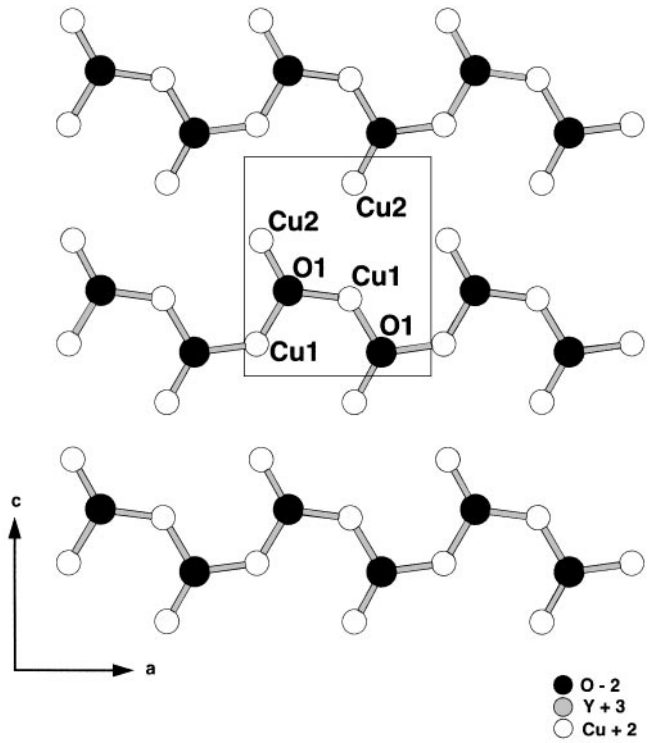

FIG. 7. Projection of the Cu–O plane ($y = \frac{1}{4}$) of $YCuO_{2.5}$ along the b-axis direction.

$P6_3/mcm$, with yttrium in 2b and 4d, copper in 6g, and oxygen in 12k ($z \approx 0.08$) and 2a positions.

The patterns in Figs. 4c or 4d can be unraveled as an overlap of the ($a_o = a_H\sqrt{3}$; $b_o = c_H$; $c_o = 2a_H$) superstructure and the ($a_H\sqrt{3}$, $a_H\sqrt{3}$, c_H) superstructure. Some of the reflections (e.g., the ones along the c_o^* direction in Fig. 4b) are mostly invisible in defective structures.

Most crystals indeed do contain defects; these are responsible for the more complex diffraction patterns in Figs. 4d–4f. Patterns such as Figs. 4d–4f show a diffuse scattering parallel to the hexagonal c^*-axis (the orthorhombic b^*-axis). This scattering is not necessarily induced by stacking errors in the basic 2H sequence, but mainly because of the presence of different orientation and translation variants of the superstructure. Since the point group of the nonoxidized phase (6/mmm) is of order 24, while the point group of the oxidized phase (mmm) is of order 8, there are obviously three orientation variants (or twin variants) possible (4). They have a common b_o axis, but the a_o and c_o axes are rotated over 60°, respectively. Such orientation variants are visible in Fig. 11. In the left (brighter) part of Fig. 11, the oxygen ordering in the Cu–O plane is clearly visible, while in a neighboring part (right side of Fig. 11) it is not visible. Orientation variants are clearly bound by $(010)_o$ and $(001)_o$ planes. Because of the four times larger unit cell of the oxidized $YCuO_{2.50}$, one can expect three different antiphase boundaries with respective displacement vectors $R_1 = \frac{1}{2}[001]$, $R_2 = \frac{1}{4}[201]$, and $R_3 = \frac{1}{4}[203]$. Such antiphase boundaries do occur, but not as frequently as twin boundaries or basic stacking faults.

Actually diffraction patterns such as Fig. 4d also result if the sample is irradiated with an intense electron beam (such as in case of high-resolution imaging). In the HREM image of Fig. 9, it is already clear that the oxygen arrangement is not equally pronounced everywhere. This is because of the degeneration of the sample with irradiation time. After a mild irradiation (enough to obtain a "normal" HREM image) a supplementary modulation with a wave vector of about 20 Å appears in the image (Fig. 12). The corresponding Fourier transform (inset of Fig. 12) is very similar to the diffraction pattern in Fig. 4d. Actually the HREM image of Fig. 12 is from the same region as the previous image in Fig. 9. This means that during electron irradiation oxygen is lost and/or redistributed, but not in a random way. The structure gradually transforms from one with oxygen content $O_{2.50}$ to one with oxygen content $O_{2.33}$. On a structural representation of the $YCuO_{2.50}$ structure, projected along the b_o-axis (Fig. 13), it is clear that some of the (100) oxygen planes will have to disappear. Actually if we number these oxygen planes, the first–second and seventh–eighth perfectly match the ($a_H\sqrt{3}$, $a_H\sqrt{3}$, c_H) superstructure. Two of the in-between planes (three–four–five–six) have to diffuse out and the remaining ones have to rearrange themselves.

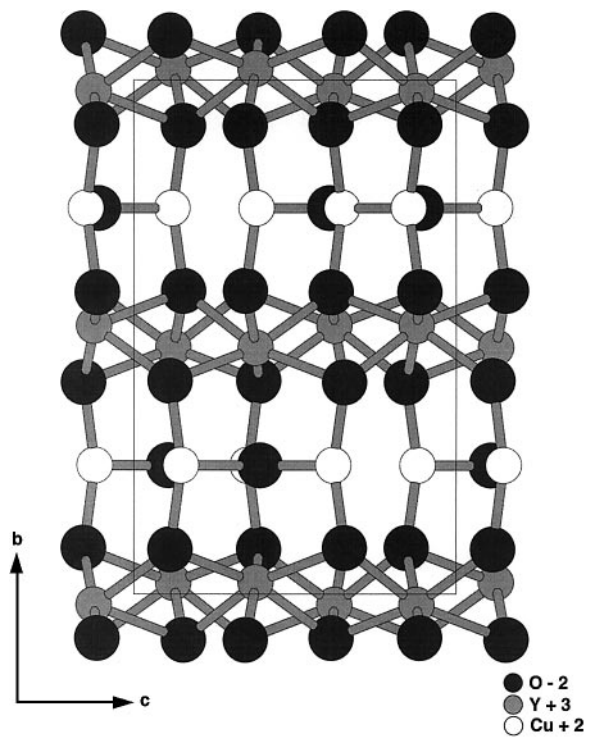

FIG. 8. Projection of the $YCuO_{2.5}$ structure along the a-axis direction.

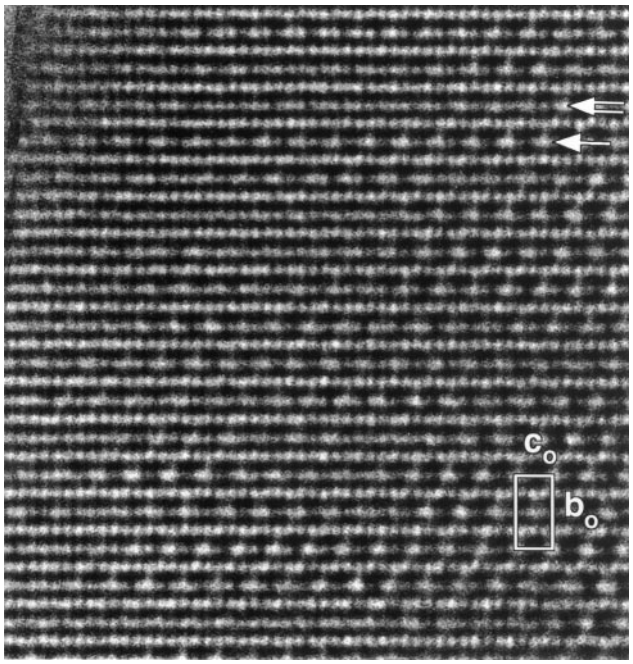

FIG. 9. $[100]_o$ HREM image, corresponding to the diffraction pattern of Fig. 5c, showing the effect of oxygen-vacancy ordering in the $CuO_{0.5}$ plane. The projected unit cell is outlined. The effect of the electron beam "damage" is clearly visible in the two equivalent rows indicated by a single and a double arrow, respectively.

The ($a_H\sqrt{3}$, $a_H\sqrt{3}$, c_H) superstructure mostly occurs in bands, bound by $(001)_H$ planes, sandwiched between the "normal" orthorhombic $YCuO_{2.50}$ structure. It looks like the stacking faults hamper the diffusion of oxygen into the structure.

Occasionally intermediate structures between the ($a_H\sqrt{3}$, c_H, $2a_H$) superstructure and the ($a_H\sqrt{3}$, $a_H\sqrt{3}$, c_H) superstructure are found. They produce even more complex and incommensurate diffraction patterns. They only occur in limited regions and will not be discussed here, but their structure can be visualized as a combination of structural arrangements of both the $YCuO_{2.50}$ structure and the $YCuO_{2.33}$ structure.

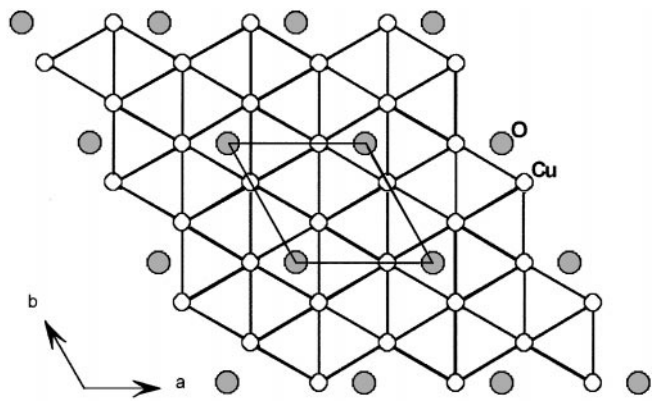

FIG. 10. Schematic representation of the hexagonal structure with ideal composition $YCuO_{2.33}$.

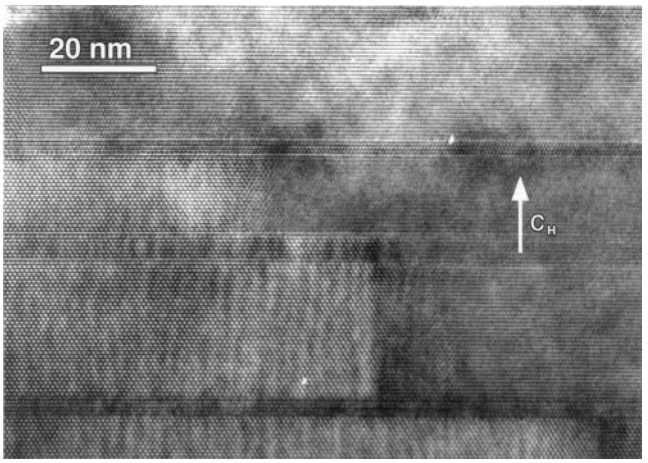

FIG. 11. HREM image at relatively low magnification showing the defect structure in a $YCuO_{2.5}$ sample; defects are primarily along $(001)_H$.

4. CONCLUSION

We have been able to produce pure $YCuO_2$ delafossite either in the hexagonal 2H or in the rhombohedral 3R form. Apparently the preparation conditions are very strict (particularly for the 3R polytype) and determine the final

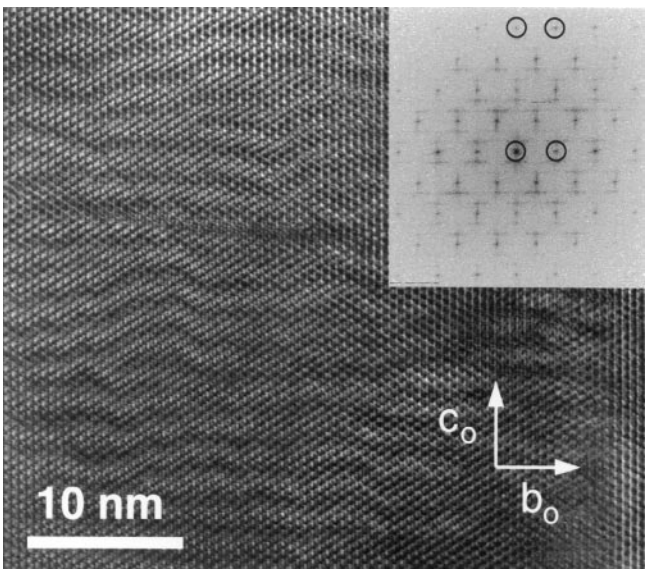

FIG. 12. HREM image of electron beam "damaged" $YCuO_{2.5}$, together with the Fourier transform of part of the image. The resemblance with the diffraction pattern of Fig. 4d is striking. The "basic" reflections in the Fourier transform are encircled.

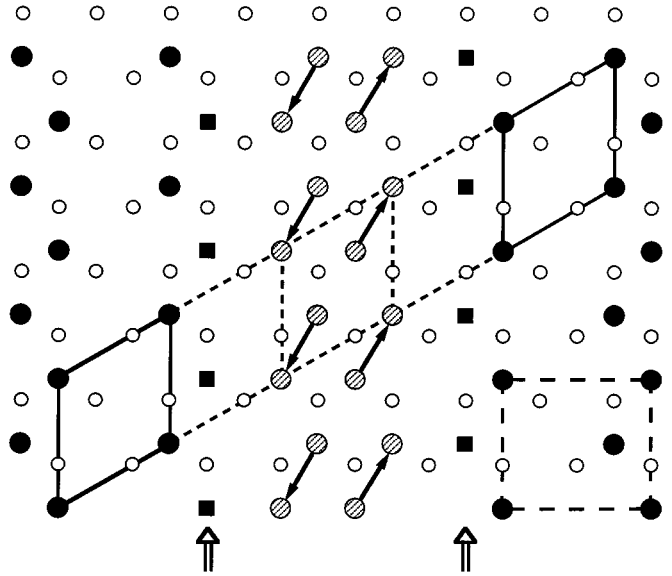

FIG. 13. Schematic representation of the Cu–O plane in $YCuO_{2.5}$ and the relation with the $YCuO_{2.33}$ structure. Larger black and gray symbols are oxygens present in the $YCuO_{2.5}$ structure. Black circles are the ones maintained in the $YCuO_{2.33}$ structure, gray ones are those to be shifted along the arrows; black squares are oxygen position no longer occupied in $YCuO_{2.33}$ and who have to diffuse out of the crystal.

structure. The fully oxygenated material $YCuO_{2.50}$ is orthorhombic with space group *Pnma* and lattice parameters $a_o = 6.1961$ Å; $b_o = 11.2158$ Å; $c_o = 7.1505$ Å and there is a very close relationship with the hexagonal 2H structure of the pure $YCuO_2$.

When the oxidation is incomplete or when the sample is irradiated by the electron beam, a related $YCuO_Z$ phase with ideal composition $YCuO_{2.33}$ and lattice parameters $a_H\sqrt{3}$, $a_H\sqrt{3}$, c_H is formed. From symmetry considerations and from the knowledge of the fully oxidized $YCuO_{2.50}$, the structure of the $YCuO_{2.33}$ phase could be determined. HREM shows evidence for a domain fragmented material as well as for oxidized states.

ACKNOWLEDGMENTS

The authors thank Dr. O. I. Lebedev for useful discussions and Dr. Eric Dooryhee for experimental help during the ESRF experiment. Part of this work was performed within the framework of IUAP 4/10.

REFERENCES

1. R. J. Cava, H. W. Zandbergen, A. P. Ramirez, H. Takagi, C. T. Chen, J. J. Krajewski, W. F. Peck Jr., J. V. Waszczak, G. Meigs, R. S. Roth, and L. F. Schneemeyer, *J. Solid State Chem.* **104,** 437 (1993); R. J. Cava, W. F. Peck Jr., J. J. Krajewski, S.-W. Cheong, and H. Y. Hwang, *J. Mater. Res.* **9,** 314 (1994); R. E. Walstedt, R. J. Cava, R. F. Bell, J. J. Krajewski, and W. F. Peak Jr., *Phys. Rev. B* **49**(17), 12,369 (1994).
2. H. Haas and E. Kordes, *Z. Kristallogr.* **129,** 259 (1969).
3. T. Ishiguro, N. Ishizawa, N. Mizutani, and M. Kato, *J. Solid State Chem.* **49,** 232 (1983).
4. A. Altomare, M. C. Burla, G. Cascarano, C. Giacovazzo, A. Guagliardi, A. G. G. Moliterni, and G. Polidori, *J. Appl. Crystallogr.* **28,** 842 (1995); A. Altomare, G. Cascarano, C. Giacovazzo, A. Guagliardi, M. C. Burla, G. Polidoiri, and M. Camalli, *J. Appl. Crystallogr.* **27,** 435 (1994).
5. J. Rodriguez-Carvajal, *Phys. B* **192,** 55 (1993).
6. N. F. Brese and M. O'Keeffe, *J. Appl. Crystallogr. B* **47,** 192 (1991).
7. G. Van Tendeloo and S. Amelinckx, *Acta Crystallogr. A* **30,** 421 (1974).